

Porous Carbon Obtained by the Pyrolysis of TiO₂/Poly(furfuryl alcohol) Nanocomposite: Preparation, Characterization and Utilization for Adsorption of Reactive Dyes from Aqueous Solution

Cláudio de Almeida Filho and Aldo J. G. Zarbin*

Departamento de Química, Universidade Federal do Paraná, CP 19081, 81531-990 Curitiba-PR, Brazil

Este trabalho descreve a preparação de carbono desordenado de alta área superficial, através da pirólise do nanocompósito TiO₂/poli(furfuril álcool). Este nanocompósito foi sintetizado pela hidrólise, em meio ácido, da mistura de isopropóxido de titânio e álcool furfurfílico. As amostras foram caracterizadas por DRX, FT-IR, espectroscopia Raman e microscopia eletrônica de transmissão. Os resultados indicaram a efetiva polimerização do FA sobre as nanopartículas de TiO₂ (forma anatase) e sua conversão a carbono desordenado após a pirólise, juntamente com a transição de fase anatase-rutilo para o TiO₂. Após a dissolução das nanopartículas do óxido com solução aquosa de HF, o carbono obtido apresentou-se extremamente poroso e com alta área superficial (700 m² g⁻¹), como uma “espuma” de carbono. Este novo material de carbono foi utilizado como adsorvente de corante azo reativo, com resultados preliminares, descritos neste trabalho, bastante satisfatórios.

This study reports the preparation of high surface area amorphous carbon by pyrolysis of TiO₂/poly(furfuryl alcohol) nanocomposite. This nanocomposite was synthesized by hydrolysis of titanium tetra-isopropoxide/furfuryl alcohol mixture. All samples were characterized by XRD, FT-IR, Raman spectroscopy and transmission electron microscopy. The results indicated the effective FA polymerization on TiO₂ (anatase) nanoparticles and polymer conversion to amorphous carbon after pyrolysis, simultaneously with TiO₂ anatase-rutile phase transition. After the oxide nanoparticles dissolution by an aqueous HF solution the obtained carbon was extremely porous, with high surface area (700 m² g⁻¹), similar to a carbon foam. With this new carbon material we carried out a study of kinetic of the adsorption of the reactive black 5 (RB5) azo-dye.

Keywords: porous carbon, nanocomposites, TiO₂, poly(furfuryl alcohol), sol-gel

Introduction

Porous carbons with a tailored pore structure represent very suitable materials for applications in several fields such as electrode materials for electric double-layer capacitors, adsorbents for gas storage, membrane separation, gas and liquid purification, catalyst supports, electrodes for lithium ion batteries, as adsorbent for color removal from industrial effluents, among others.¹⁻⁶

Many novel approaches to control the pore structure of several kinds of porous carbons have been proposed. One of the most important techniques is the template carbonization method, based on the carbonization of an organic polymer in some inorganic host material.^{2,7-12} The

general procedure consists of preparing a (nano)composite using the polymer and the inorganic material, followed by the carbonization. The resulting inorganic/carbon (nano)composite is subsequently treated with an adequate solution in order to dissolve the inorganic fraction and the carbon template is obtained as the insoluble product. At the moment, the template technique for novel carbon materials has been carried out using a combination of different precursors and inorganic hosts.^{2,7-12}

Several different organic polymers have been used as carbonaceous precursor.¹³⁻¹⁵ Among them, poly(furfuryl alcohol) (PFA) is a common typical thermosetting resin that forms carbon with a fairly high yield on carbonization.¹⁶⁻¹⁸ PFA can be easily formed from its monomer liquid (furfuryl alcohol – FA) in which acid is added as a catalyst for polymerization. The carbonization reactions of PFA and the properties of the carbon materials derived

*e-mail: aldo@quimica.ufpr.br

from it have been investigated in a great deal for several decades.¹⁶⁻¹⁸ The synthesis of porous carbon from PFA/porous silica glass nanocomposite was recently reported by our research group.^{19,20}

This work describes the synthesis and characterization of novel porous carbon material from the pyrolysis of TiO₂/poly(furfuryl alcohol) nanocomposite obtained by the sol-gel method, and the initial results regarding the use of this carbon material as adsorbent of a reactive azo-dye from aqueous solution.

Experimental

Materials

Furfuryl alcohol (FA) was obtained from Merck and purified by distillation. The water employed in all preparations was distilled and deionized by a Milli-Q system (Millipore). All the other chemicals were used as received. Titanium tetra-isopropoxide (TTIP) was purchased from Strem. Hydrochloric acid and 2-propanol were purchased from Carlo Erba. Aqueous hydrofluoric acid solution (48 wt%) was obtained from Nuclear. Reactive black 5 (RB5) dye was supplied from Aldrich.

Preparation of nanocomposite TiO₂/PFA

The synthetic procedure for our TiO₂/poly(furfuryl alcohol) nanocomposites is similar to the approach described by our research group for TiO₂/polyaniline nanocomposites,²¹ based on addition of the FA monomer on a TTIP solution before the hydrolysis step in which the TiO₂ nanoparticles will be formed. The experiment can be described as follows: in a glove-box, 1.69 mL of FA was added to a solution formed by 2.0 mL of TTIP and 2.0 mL of 2-propanol (TTIP/FA molar ratio = 1:2.9). Instantly the colorless TTIP solution turned into a red translucent one. This solution was mixed with 12.0 mL of a 0.2 mol L⁻¹ HCl aqueous solution. Precipitation occurred immediately. The mixture was maintained under magnetic stirring for 8 h at 60 °C in a reflux system. The resulting mixture was dark-brown indicating the formation of oligomers and polymers of FA. Water and solvent were subsequently removed under vacuum at 40 °C, resulting in a brown powder that will be referred to as TiO₂/FA.

For comparison, a neat TiO₂ sample was prepared by an acidic hydrolysis of TTIP, in a similar procedure as described before but without the addition of FA. After the drying step, the white powder obtained should be considered as a TiO₂ xerogel, and will be referred to as TiO₂-X.

The TiO₂/FA sample was processed by thermal treatment at 70 °C for 24 hours to promote the whole FA polymerization. This new dark-brown powder sample will be mentioned as TiO₂/PFA.

Preparation of porous carbon

The TiO₂/PFA sample was pyrolyzed at 900 °C under argon flow. Approximately 0.2 g of this sample was put in a tubular furnace at room temperature. A flow of 260 mL min⁻¹ of argon was continuously passed over the furnace and the temperature was raised until 900 °C at a rate of 10 °C min⁻¹. The sample remained at 900 °C by 2 hours. After this, the temperature was decreased until room temperature. The resulting sample becomes black and will be referred to as TiO₂/C.

The TiO₂/C sample was treated with HF solution in order to remove the TiO₂ by dissolution. The HF treatment was carried out adding approximately 0.05 g of TiO₂/C sample to 30.0 mL of aqueous HF solution (hazardous) for a week. The resulting insoluble material, referred to as C sample, was retrieved by centrifugation, washed exhaustively with H₂O and dried at 50 °C for 24 hours.

Batch kinetic study

The kinetic experiment was performed by the batch method. The RB5 azo-dye was diluted in water at the initial concentration (C₀) of 100 mg L⁻¹ (pH = 5.6) of the dyestuff. An amount of 0.015 g of C sample was added to 50 mL of the dye solution and maintained under magnetic stirring at 29 °C. Several aliquots of the mixture were collected at different times, filtered through a Millipore membrane filter and the concentration of dye in solution was determined by UV-Vis spectroscopy.

Apparatus

The FT-IR spectra of the samples were obtained with a Bio-Rad (Excalibur FTS 3500GX) spectrophotometer in the 4000 to 400 cm⁻¹ range with 32 scans and resolution of 4 cm⁻¹. The samples were prepared in KBr pellets.

The X-ray diffraction (XRD) patterns were taken in a Shimadzu (XRD-6000) diffractometer using Cu K_α radiation (λ = 1.5418 Å) at 40 keV and 40 mA. The diffractograms were collected at a rate of 2° min⁻¹.

The Raman spectra were obtained in a Renishaw spectrophotometer coupled to an optical microscope that focuses the incident radiation down to an approximately 1 μm spot. An argon laser (λ = 514.5 nm) was used with 20 mW incidence potency over the 200-4000 cm⁻¹ region.

The specific surface area was determined by the BET technique in a Flowsorb II 2300 equipment.

The concentrations of RB5 dye in solution were obtained using a UV-Visible spectrophotometer (Hewlett-Packard, 8452A). The maximum absorption values were obtained at 594 nm.

The transmission electronic microscopy (TEM) analysis was performed in a Jeol (Jem 1200 EXII, 120 KeV) microscope. The samples were suspended in *N,N*-dimethylformamide (DMF) and a drop of the supernatant dispersion was placed onto a sample holder (formed by a carbon film supported by a copper grid).

Results and Discussion

Characterization of the materials

It is well known that poly(furfuryl alcohol) can be formed from furfuryl alcohol monomer by acid catalysis and heating. The synthetic route used in this work aims at the formation of both TiO₂ nanoparticles and PFA in a single experiment, looking for an intimate contact between the polymer and the oxide nanoparticles, which should result in a highly porous carbon after the pyrolysis and oxide dissolution. When the TTIP/FA mixture was added to the HCl aqueous solution, the hydrolysis of TTIP occurs immediately and the acidic medium starts the FA polymerization. The heat treatment at 60 °C makes the polymerization quickly and promotes the TiO₂ peptization. After the solvent removal, the powder sample was further heat-treated in order to guarantee the furfuryl alcohol complete polymerization. The polymer formation was evidenced by the strong brown color observed on the TiO₂/PFA sample, similar to that of neat PFA resin.

Figure 1 shows the infrared spectra of the samples TiO₂-X, TiO₂/PFA, TiO₂/C and C. A spectrum of a neat PFA sample was added on the Figure for comparison. The spectrum of the TiO₂-X sample (Figure 1a) presents one band at 3233 cm⁻¹ due to the stretching of OH groups from the adsorbed water and from residual surface OH groups; one band at 1618 cm⁻¹ attributed to the H-O-H bending due to the adsorbed water, and one band at 596 cm⁻¹ due the Ti-O stretching and Ti-O-Ti bending, characteristic of the anatase structure of TiO₂.^{22,23}

The spectrum of TiO₂/PFA sample (Figure 1b) shows, besides the bands attributed to TiO₂ discussed before, a series of novel bands, all of them characteristics of the PFA, as can be observed by comparison between this spectrum and the spectrum of a neat PFA sample, shown in Figure 1c.²⁴⁻²⁶ A detail on the region of the main PFA bands is shown in Figure 1(II). The assignment of the

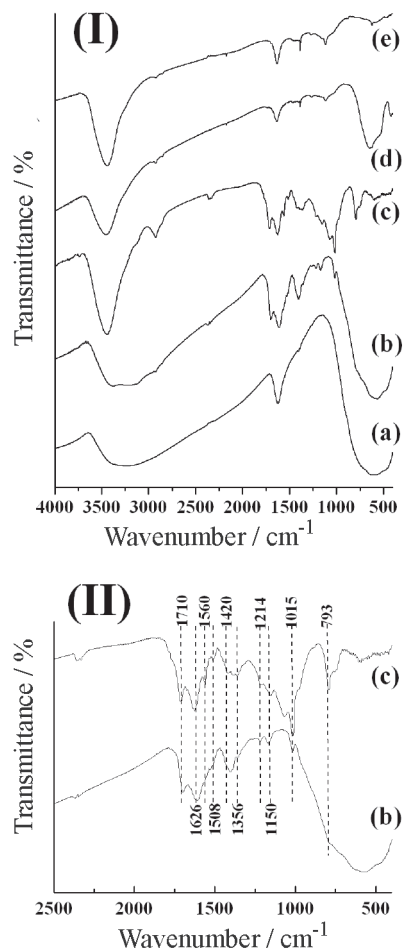


Figure 1. (I) FT-IR spectra of samples: (a) TiO₂-X; (b) TiO₂/PFA; (c) neat PFA; (d) TiO₂/C; (e) C. (II) detail (2500 to 400 cm⁻¹) of the spectra of the samples TiO₂/PFA (b) and neat PFA (c).

main PFA bands observed on the spectrum of the TiO₂/PFA sample is the following: ν C-H (2928 cm⁻¹), ν C=O (1710 cm⁻¹), ν C=C (1560 cm⁻¹), ν C=C (1508 cm⁻¹), δ C-C-O, CH₂ (1420 cm⁻¹), ν C=C (1356 cm⁻¹), ν C-OH, ν C-OC (1214 cm⁻¹), δ C-C-H (1150 cm⁻¹), ν C-O (1015 cm⁻¹), δ C-C-H (793 cm⁻¹). The band at 1710 cm⁻¹ is attributed to the aliphatic diketone C=O stretching. Several authors have detected the presence of aliphatic diketone species in the PFA structure, formed due to the opening of a furan ring by the acid catalyzed electrophilic attack of water molecules, formed as a by-product of the polymerization of FA.²⁴⁻²⁶

The TiO₂/C spectrum (Figure 1d) shows two well defined bands at 646 cm⁻¹ and 552 cm⁻¹ attributed to TiO₂ in the rutile form, which is the first evidence that the thermal treatment of the TiO₂/PFA samples causes a phase transition in the oxide nanoparticles. This statement will be discussed latter. There are no bands in this spectrum that could be attributed to PFA, suggesting the complete

pyrolysis of the polymer. The spectrum of the C sample (Figure 1e) shows that the rutile dissolution by HF treatment was complete since there are no bands attributed to this oxide, indicating only residual insoluble carbon.

Figure 2 presents the X-ray diffractograms of the TiO_2 -X (Figure 2a), TiO_2 /PFA (Figure 2b), TiO_2 /C (Figure 2c) and C (Figure 2d) samples. According to Figure 2a, the TiO_2 -X is formed mainly in the anatase structure (those peaks are marked with an A in Figure 2) with traces of brookite (peaks marked with B in the Figure 2). The XRD pattern of the TiO_2 /PFA sample (Figure 2b) presents the same profile observed in the pure oxide, indicating that the structure of the oxide was not modified by the poly(furfuryl alcohol). The diffractogram of this sample presents also a noticeable amorphous halo due the polymer in the sample. The broad peak observed in the XRD profile of both TiO_2 -X and TiO_2 /PFA samples indicates small crystallite diameter of the oxide, which was estimated by the Scherrer's equation as approximately 4.0 nm.

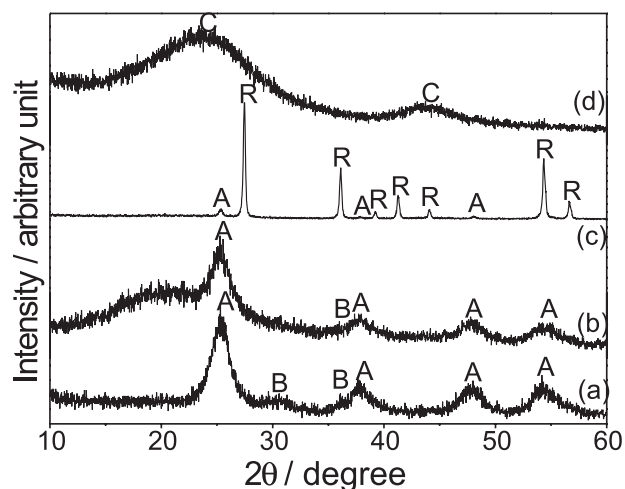


Figure 2. X-ray diffractograms of samples: (a) TiO_2 -X; (b) TiO_2 /PFA; (c) TiO_2 /C; (d) C. A = anatase, B = brookite, R = rutile, C = carbon.

The pyrolysis of the TiO_2 /PFA sample makes the transition from anatase and brookite to rutile phase, as observed in the XRD pattern of TiO_2 /C sample in Figure 2c. However this transition is not complete at the pyrolysis setup employed here. The remainder anatase phase (observable by the XRD profile present on Figure 2c) probably indicates the large PFA amount present on the nanocomposite interfered in the anatase-rutile phase transition kinetic, once the same pyrolysis conditions applied to the TiO_2 -X sample carried out to a complete conversion of the oxide to the rutile phase (data not shown).

After the oxide dissolution by HF treatment, the resulting C sample presents the XRD pattern shown in Figure 2d, which shows two broad peaks associated with the (002) and (10) reflections from graphite. The

interplanar space (d_{002}) calculated to this sample is 4.05 Å, larger than the observed to graphite (3.354 Å) indicating considerable disordered carbon. The d_{002} value is traditionally used to estimate a graphitization degree of the carbon. In general, growing disorder in the carbon materials is reflected in increased values of d_{002} .²⁷⁻²⁹ The absence of any peak related to the TiO_2 is an indicative that all oxide was dissolved from the HF treatment.

The samples were also characterized by Raman spectroscopy, and the spectra are presented in Figure 3. Unfortunately we were not able to collect the Raman spectra of the TiO_2 /PFA sample due to the strong fluorescence observed on this sample. The spectrum of the TiO_2 -X sample (Figure 3a) presents bands that should be attributed to TiO_2 in both anatase and brookite phase, confirming the XRD data that showed that the titanium oxide was formed in these two polymorphs.³⁰ The phase transition to rutile after the thermal treatment was also confirmed by Raman spectroscopy, according to the spectrum of the TiO_2 /C sample present in the Figure 3b.³¹ However, besides the rutile bands (marked with a R in the spectrum), it is noticeable the occurrence of two new bands in the TiO_2 /C spectrum, at 1591 and 1336 cm^{-1} . These bands are the so-called G and D bands, respectively, and are characteristic of disordered carbon materials. After the TiO_2 dissolution, only these two carbon-bands remain in the Raman spectrum of the C sample (Figure 3c), confirming that all the oxide dissolution was effective and the resulting material is a disordered carbon. Note that all information extracted from the Raman spectra of the samples is in perfect agreement with that supplied by XRD.

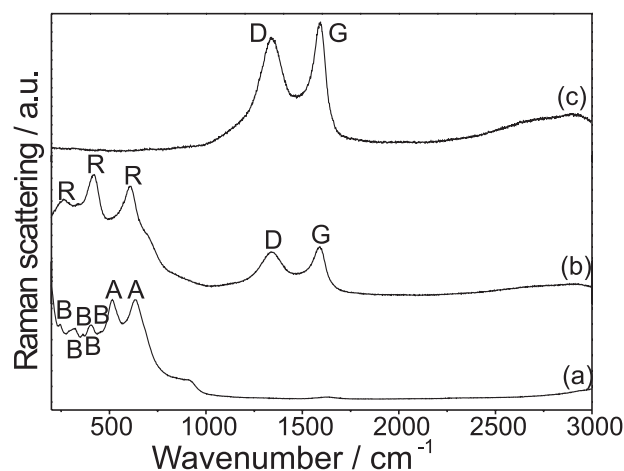


Figure 3. Raman spectra of samples: (a) TiO_2 -X; (b) TiO_2 /C; (c) C. A = anatase, B = brookite, R = rutile, D = carbon D line, G = carbon G line.

Raman spectroscopy is a very useful characterization tool for carbon materials. For a single crystal of graphite, two Raman modes can be observed at 1582 (the stretching

mode of individual sheets, called G-line) and 42 cm^{-1} (the shear mode of two adjacent sheets).^{29,32,33} In disordered carbons, the shear mode disappears; the G line becomes broad and is shifted to as far as 1600 cm^{-1} (depending on the type of material and the degree of disorder), and another broader line appears at $\sim 1360\text{ cm}^{-1}$. This new band (called D-line, where D stands for disorder) is an in-plane mode which becomes active by small imperfections due to the particle size effect and the loss of translational symmetry in the disordered structure.^{28,29,32,33} The width and relative intensities of both G and D lines (I_D/I_G) vary with the ordering of the structure and may be used to characterize carbon materials (in general, a lower I_D/I_G ratio can be correlated with a lower disorder degree).^{28,29,32,33} As described before, the Raman spectrum of the C sample presents only the D and G carbon lines. The D band is intense and wide, and the estimated I_D/I_G was 2.09, confirming that, as observed before by XRD, the obtained carbon is substantially disordered.

The TiO_2/C and C samples were analyzed by transmission electronic microscopy (TEM) and the images are shown in Figures 4 and 5. As we can see in Figure 4, the TiO_2/C sample is formed by great agglomerates with several dark points inside. Because this sample is composed by both TiO_2 nanoparticles and carbon (according the XRD and Raman results showed before), we suppose that the dark points should correspond to the TiO_2 nanoparticles (higher contrast), embedded in a mass that should correspond to the carbon resulting from the PFA. The images present in Figure 4 indicate that there is no phase segregation, and carbon and oxide phases are intimately mixed together. This should be due to the high oxide/polymer affinity achieved in the TiO_2/PFA sample, as result of the preparation method developed in this work. As the oxide nanoparticles are supposed homogeneously dispersed in the carbon mass, after the oxide dissolution the resulting C sample presents a homogeneous dispersion of pores in a carbon mass, as observable in the TEM images present on Figure 5, resulting in a high porous carbon with structures that remind a carbon foam. The BET specific surface measured for this sample was $700\text{ m}^2\text{ g}^{-1}$.

Adsorption kinetics

Adsorption is an efficient and economically feasible process for the treatment of wastewater containing chemically stable pollutants such as reactive dyes. By this way, the porous carbon material obtained in this work was used as adsorbent for Reactive black 5 (RB5), an anionic reactive dye. Kinetic data were analyzed using

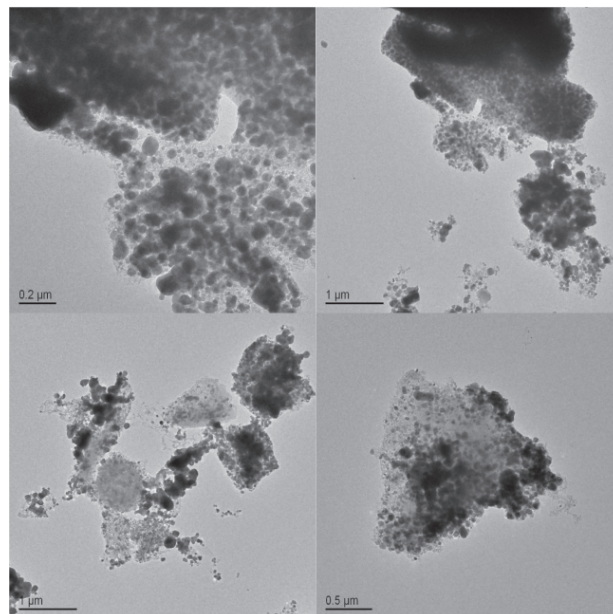


Figure 4. TEM images of the TiO_2/C sample.

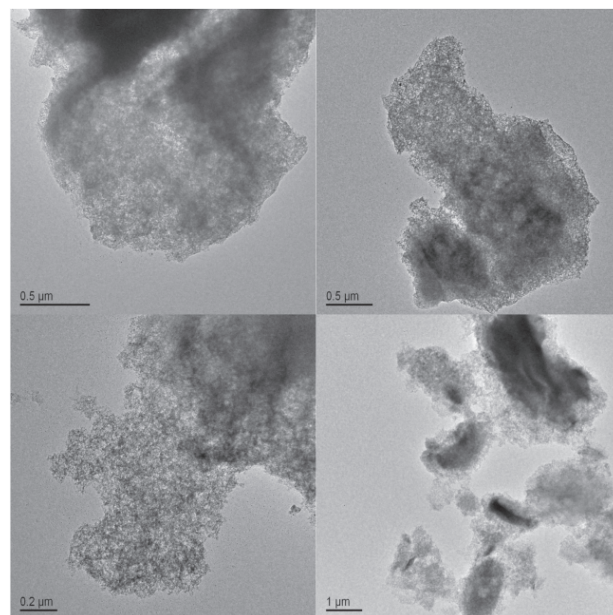


Figure 5. TEM images of the C sample.

the pseudo first-order (equation 1), the pseudo second-order (equation 2) and the intraparticle diffusion (equation 3) equations:³⁴

$$\log(q_e - q) = \log q_e - \frac{k_1}{2.303} t \quad (1)$$

$$\frac{t}{q} = \frac{1}{k_2 q_e^2} + \frac{t}{q_e} \quad (2)$$

$$q = k_p t^{1/2} \quad (3)$$

where t is time (min), q_e is the amount of RB5 adsorbed

at equilibrium (mg g^{-1}), q is the amount of RB5 adsorbed at time t (mg g^{-1}), k_1 is the rate constant of first-order adsorption (min^{-1}), k_2 is the rate constant of second-order adsorption ($\text{g mg}^{-1} \text{min}^{-1}$) and k_p is the intraparticle rate constant ($\text{mg g}^{-1} \text{min}^{-1/2}$).

Figure 6 shows the adsorption isotherm of the experiment, in which the adsorption equilibrium was attained near 480 min. The amount of RB5 adsorbed at equilibrium (q_e) was 61.90 mg g^{-1} . This q_e value is considered very satisfactory when compared with previous published results of maximum adsorption capacity of activated carbon.³⁵

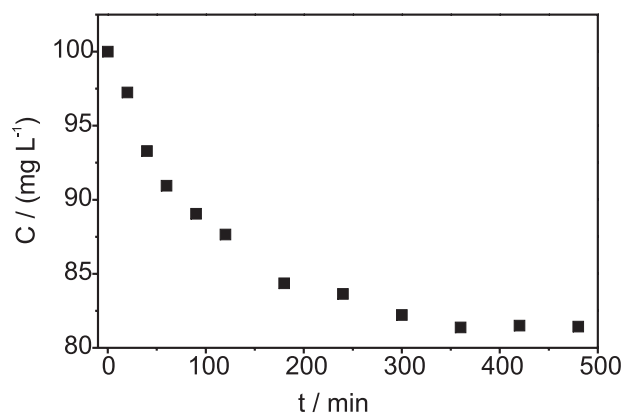


Figure 6. Isotherm of adsorption of RB5 from aqueous solution by C sample.

For the purpose to quantifying the changes in the adsorption of RB5 with time we tested three kinetic models. First of all, the pseudo first-order equation (equation 1) was applied. Figure 7 shows that the adsorption of the dye followed this kinetic modeling only in the initial stage. From the slope of the linear plot in the initial stage, shown in the inset of the Figure 7, the value of first-order rate constant k_1 was evaluated to be $9.95 \times 10^{-3} \text{ min}^{-1}$.

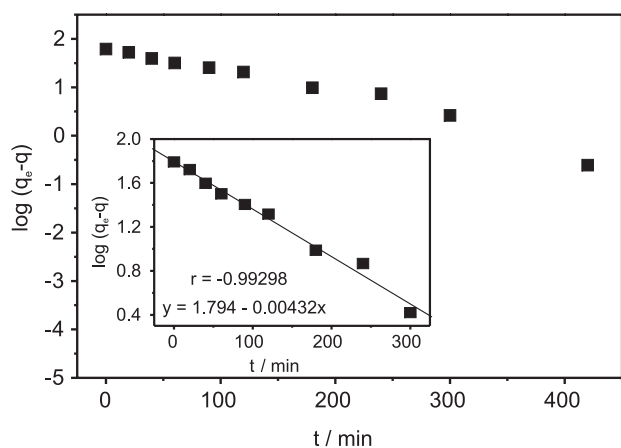


Figure 7. Plot of the pseudo first-order model of kinetic curve related to the absorption of RB5 from aqueous solution by C sample.

The kinetics of adsorption of RB5 onto sample C was also evaluated by applying the pseudo second-order equation (equation 2). Figure 8 shows that adsorption followed well this model over the entire range of stirring time explored. The rate constant of second-order was evaluated as $k_2 = 1.89 \times 10^{-4} \text{ g mg}^{-1} \text{ min}^{-1}$.

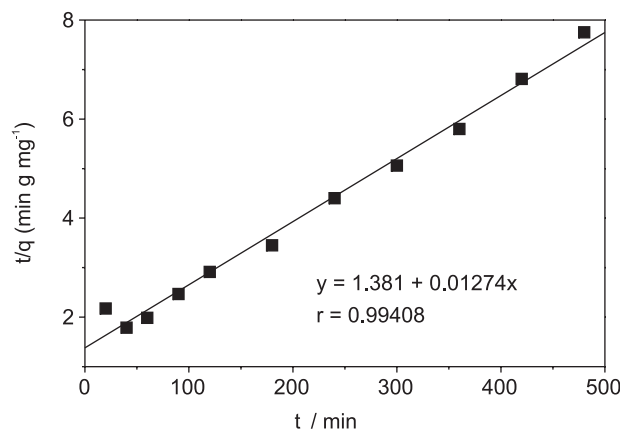


Figure 8. Plot of the pseudo second-order model of kinetic curve related to the absorption of RB5 from aqueous solution by C sample.

Figure 9 presents the kinetics of adsorption by the intraparticle diffusion equation (equation 3) that indicates the transport mechanisms of the solute. The plot can be divided in three sections. The two initial plot sections can be seen in the inset of the Figure 9 with a fit straight line passing through the origin. The first initial portion is curved and this deviation can be attributed to boundary layer diffusion effects. The second plot portion is linear with the origin due the intraparticle diffusion of the RB5. In this range, intraparticle diffusion mechanisms are involved in the adsorption rate:³⁴ (i) diffusion within the pore volume and (ii) diffusion along the surface of the pores. Both pore diffusion and surface mechanisms occur in parallel within the C sample and control the adsorption

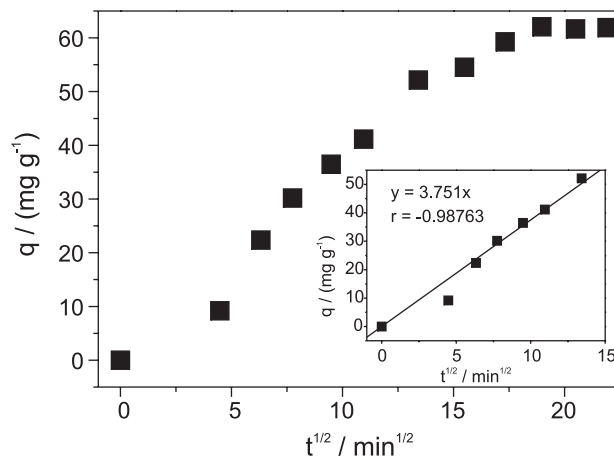


Figure 9. Plot of the intraparticle diffusion model of kinetic curve related to the absorption of RB5 from aqueous solution by C sample.

kinetics. The intraparticle transport rate constant, $k_p = 3.75 \text{ mg g}^{-1} \text{ min}^{1/2}$, is the slope of the fit straight line that pass through the origin. The third portion of the plot shows the deviation of this model when q approaches to q_c .

Conclusions

In this study we have prepared novel $\text{TiO}_2/\text{poly}(\text{furfuryl alcohol})$ nanocomposite, based on the sol-gel process, that was used as precursor for a high porous carbon material, obtained from the pyrolysis of the nanocomposite followed by the dissolution of the oxide fraction. The characterization data presented in this work provide evidences that the characteristics of the final material are strongly related with the adopted synthetic route to the oxide/polymer nanocomposite. The high porosity and high surface area displayed by the carbon material described here make it suitable for a many applications, such as sorbents or materials for carbon electrodes. The experimental results of the kinetics of the adsorption indicate that this material can be used as adsorbent in exhaustive adsorption studies of dyestuffs. Further studies on this direction, including adsorption kinetics with different cationic, neutral and anionic dyes, are currently been done in our laboratory.

Acknowledgments

This work was supported by CNPq, CT-ENERG/CNPq, TWAS, Rede de Materiais Nanoestruturados and Rede Nacional de Nanotubos (MCT/CNPq). Authors thank Dr. Marcela M. Oliveira and Centro de Microscopia Eletrônica–UFPR for the TEM images, and Prof. Yoshitaka Gushiken (IQ-UNICAMP) for the BET analysis. CAF greatly acknowledges the postdoctoral fellowship provided by CNPq.

References

1. Ma, Z.; Kyotani, T.; Tomita, A.; *Chem. Commun.* **2000**, 2365.
2. Sakintuna, B.; Yürüm, Y.; *Ind. Eng. Chem. Res.* **2005**, *44*, 2893.
3. Wen, Y.; Cao, G.; Yang, Y.; *J. Power Sources* **2005**, *148*, 121.
4. Garsuch, A.; Sattler, R.R.; Witt, S.; Klepel, O.; *Microporus Mesoporus Mat.* **2006**, *89*, 164.
5. Vu, D.Q.; Koros, W.J.; Miller, S.J.; *J. Membr. Sci.* **2003**, *211*, 311.
6. Wang, Q.; Li, H.; Chen, L.Q.; Huang, X.J.; *Solid State Ionics* **2002**, *152*, 43.
7. Kyotani, T.; Yamada, H.; Sonobe, N.; Tomita, A.; *Carbon* **1994**, *32*, 627.
8. Kawashima, D.; Aihara, T.; Kobayashi, Y.; Kyotani, T.; Tomita, A.; *Chem. Mater.* **2000**, *12*, 3397.
9. Ma, Z.; Kyotani, T.; Liu, Z.; Terasaki, O.; Tomita, A.; *Chem. Mater.* **2001**, *13*, 4413.
10. Ania, C. O.; Bandosz, T. J.; *Microporus Mesoporus Mat.* **2006**, *89*, 315.
11. Garsuch, A.; Klepel, O.; Sattler, R.R.; Berger, C.; Glaser, R.; Weitkamp, J.; *Carbon* **2006**, *44*, 596.
12. Wang, H.; Li, X.; Hong, L.-Y.; Kim, D.-P.; *J. Porous Mat.* **2006**, *13*, 115.
13. Johnson, D. J.; Crawford, D.; Oates, C.; *Carbon* **1972**, *10*, 330.
14. Ohnishi, T.; Murase, I.; Noguchi, T.; Hirooka, M.; *Synth. Met.* **1986**, *14*, 207.
15. Bürger, A.; Fitzer, E.; Heym, M.; Terwiesch, B.; *Carbon* **1975**, *13*, 149.
16. Zhang, X. Q.; Solomon, D. H.; *Chem. Mater.* **1999**, *11*, 384.
17. Wang, Z.; Lu, Z.; Huang, X.; *Carbon* **1998**, *36*, 51.
18. Bandosz, T. J.; Jagiello, J.; Putyera, K.; Schwarz, J. A.; *Langmuir* **1995**, *11*, 3964.
19. Zarbin, A. J. G.; Bertholdo, R.; Oliveira, M. A. F. C.; *Carbon* **2002**, *40*, 2413.
20. Zimmer, A. M.; Bertholdo, R.; Grassi, M. T.; Zarbin, A. J. G.; Mascaro, L. H.; *Electrochem. Commun.* **2003**, *5*, 983.
21. Schnitzler, D. C.; Meruvia, M. S.; Hümmelguen, I. A.; Zarbin, A. J. G.; *Chem. Mater.* **2003**, *15*, 4658.
22. Lopez, T.; Sanchez, E.; Bosch, P.; Meas, Y.; Gomez, R.; *Mater. Chem. Phys.* **1992**, *32*, 141.
23. Sanchez, E.; Lopez, T.; Gomez, R.; Bokhimi; Morales, A.; Novaro, O.; *J. Solid State Chem.* **1996**, *122*, 309.
24. Shindo, A.; Izumino, K.; *Carbon* **1994**, *32*, 1233.
25. Conley, R. T.; Metil, I.; *J. Appl. Polym. Sci.* **1963**, *7*, 37.
26. Milkovic, J.; Myers, G. E.; Young, R. A.; *Cellul. Chem. Technol.* **1979**, *13*, 651.
27. Kyotani, T.; Nagai, T.; Inoue, S.; Tomita, A.; *Chem. Mater.* **1997**, *9*, 609.
28. Cuesta, A.; Dhamelincourt, P.; Laureyns, J.; Martínez-Alonso, A.; Tascón, J. M. D.; *J. Mater. Chem.* **1998**, *8*, 2875.
29. Wang, Z.; Lu, Z.; Huang, Y.; Xue, R.; Huang, X.; Chen, L.; *J. Appl. Phys.* **1997**, *82*, 5705.
30. Hu, Y.; Tsai, H.-L.; Huang, C.-L.; *J. Eur. Ceram. Soc.* **2003**, *23*, 691.
31. Falaras, P.; Goff, A. H.-L.; Bernard, M. C.; Xagas, A.; *Sol. Energy Mater. Sol. Cells* **2000**, *64*, 167.
32. Tuinstra, F.; Koenig, J. L.; *J. Chem. Phys.* **1970**, *53*, 1126.
33. Wang, Z.; Lu, Z.; Huang, X.; Xue, R.; Chen, L.; *Carbon* **1998**, *36*, 51.
34. Uzun, I.; *Dyes Pigm.* **2006**, *70*, 76.
35. Al-Degs, Y.; Khraisheh, M.A.M.; Allen, S. J.; Ahmad, M.N.A.; *Adv. Environ. Res.* **1999**, *3*, 132.

Received: March 14, 2006

Published on the web: August 30, 2006